Solar Phys (2021) 296:33
https://doi.org/10.1007/s11207-021-01774-9

Weakest Solar Cycle of the Space Age: A Study on Solar Wind–Magnetosphere Energy Coupling and Geomagnetic Activity

Rajkumar Hajra[1]

Received: 21 September 2020 / Accepted: 19 January 2021

Abstract Solar Cycle 24, from December 2008 to December 2019, is recorded to be the weakest in magnitude in the space age (after 1957). A comparative study of this cycle with Solar Cycles 20 through 23 is presented. It is found that Solar Cycle 24 is not only the weakest in solar activity, but also in average solar wind parameters and solar wind–magnetosphere energy coupling. This resulted in lower geomagnetic activity, lower numbers of high-intensity long-duration continuous auroral electrojet (AE) activity (HILDCAA) events and geomagnetic storms. The Solar Cycle 24 exhibited a $\approx 54-61\%$ reduction in HILDCAA occurrence rate (per year), $\approx 15-34\%$ reduction in moderate storms (-50 nT $\geq Dst > -100$ nT), $\approx 49-75\%$ reduction in intense storms (-100 nT $\geq Dst > -250$ nT) compared to previous cycles, and no superstorms ($Dst \leq -250$ nT). Implications of the solar and geomagnetic weakening to space weather science and operations are discussed.

Keywords Solar cycle · Solar wind–magnetosphere coupling · Magnetic storms · Substorms · HILDCAAs

1. Introduction

The recently complete Solar Cycle 24 was the weakest in magnitude in the space exploration era, i.e. after 1957. The solar cycle extending from December 2008 to December 2019 had a maximum smoothed sunspot number (SSN) of 116 recorded during April 2014, significantly low compared to previous Solar Cycles 20 through 23 with maximum SSNs of 157, 233, 214, and 180, respectively. The reduction in solar activity is extensively studied (see, e.g., Janardhan, Bisoi, and Gosain, 2010; Tsurutani, Echer, and Gonzalez, 2011; Livingston, Penn, and Svalgaard, 2012; Janardhan et al., 2015; Sasikumar Raja et al., 2019, and references therein), and is attributed to a steady declining of the solar photospheric magnetic fields (at solar latitudes $\geq 45°$) since $\approx$1995. In addition, Janardhan et al. (2018) reported

✉ R. Hajra
rajkumarhajra@yahoo.co.in

[1] Indian Institute of Technology Indore, Simrol, Indore 453552, India

a $\approx$ 2.5-year gap between the field reversals in the two solar hemispheres around the maximum of Solar Cycle 24, which is an unusual and unprecedented hemispheric asymmetry.

Ingale, Janardhan, and Bisoi (2019), using numerical and empirical models, showed an increasing trend in the Earth's magnetopause and bow shock stand-off distances as a consequence of the declining solar magnetic fields. Kakad et al. (2019) performed a detailed analysis of the impact of the decreasing solar activity on the terrestrial magnetosphere-ionosphere system. Substantial weakening of the energy coupling was shown to result in significant decreases in the ring current, auroral and equatorial ionospheric electrojet currents in Solar Cycle 24 compared to Solar Cycles 22 and 23. Grandin, Aikio, and Kozlovsky (2019) reported a similar decrease in the geoeffectiveness of solar wind high-speed streams (HSSs) in terms of lower ring current and auroral electrojet current values during Solar Cycle 24 than in Solar Cycle 23.

The aim of the present work is to study the geomagnetic characteristics of Solar Cycle 24 in comparison to all previous cycles in the space exploration era (after 1957). The geomagnetic activity at Earth is caused by solar wind–magnetosphere energy coupling through the process of magnetic reconnection (Dungey, 1961; Gonzalez and Mozer, 1974). Strong and long-duration magnetic reconnection may lead to enhanced (westward) ring current resulting in global-scale geomagnetic depressions commonly known as magnetic storms (Gonzalez et al., 1994). Auroral substorms (Akasofu, 1964) are caused by precipitation of energetic ions and electrons in the auroral ionosphere in the process of discrete and weaker reconnection (Tsurutani and Meng, 1972; Ohtani, 2001). Intense auroral substorms continuing for a few days without any significant magnetic storm have been called high-intensity long-duration continuous auroral electrojet (AE) activity (HILDCAA; Tsurutani and Gonzalez, 1987; Hajra et al., 2013). Magnetic storms, substorms and HILDCAAs are associated with varying solar-interplanetary drivers during different phases of the solar cycle (see Hajra, Tsurutani, and Lakhina, 2020; Tsurutani, Lakhina, and Hajra, 2020, for reviews of drivers). In the present work, the impact of the reduced solar activity during Solar Cycle 24 on the solar wind–magnetosphere energy coupling and in resulting geomagnetic activity will be assessed. While some of the above cited works studied geoeffectiveness in terms of ring current and auroral electrojet current, variations of HILDCAAs and magnetic storms of varying intensity during Solar Cycle 24 in comparison to previous cycles have not been reported before. The latter is the main focus of the present work. As a reduced solar activity will cause a higher flux of cosmic rays in near-Earth space, such a study can have broader implications on manned missions at low Earth orbit or to the Moon and Mars.

2. Data Analysis and Results

Figure 1 shows monthly (black) and yearly (red) mean smoothed sunspot numbers (SSNs), cosmic ray (CR) count rates recorded at Oulu, Finland, and geomagnetic indices Dst, ap, and AE for the period from 1963 through 2019. It covers five complete solar cycles (SCs): SC20, SC21, SC22, SC23, and SC24. Details of the cycle properties are given in Table 1. The SSN data and the CR counts are obtained from the Royal Observatory of Belgium, Brussels (http://www.sidc.be/silso/home), and the Sodankyla Geophysical Observatory, University of Oulu (http://cosmicrays.oulu.fi/), respectively. The geomagnetic indices are collected from the World Data Center for Geomagnetism, Kyoto, Japan (http://wdc.kugi.kyoto-u.ac.jp/index.html).

From SC21 through SC24, a clear decreasing trend can be noted in the cycle amplitude. The CR exhibits prominent anti-correlation (correlation coefficient $r = -0.81$ and -0.87

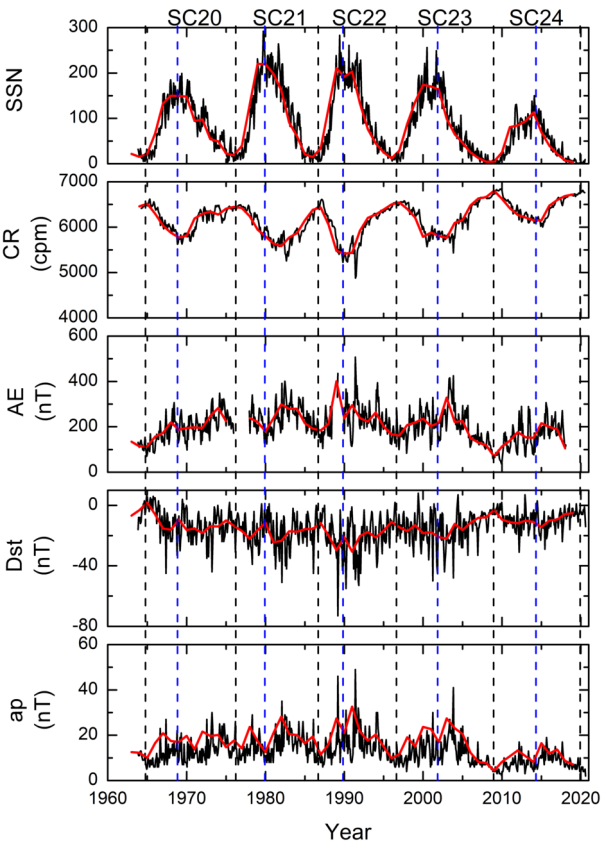

Figure 1 From top to bottom, the panels show the smoothed sunspot numbers (SSNs), Finland cosmic ray (CR) count rate, geomagnetic AE, Dst, and ap indices. In each panel, black and red curves show the monthly mean and yearly mean values of the parameters, respectively. Dashed vertical blue and black lines indicate the SSN maximum and minimum, respectively. Solar cycles (SCs) from SC20 through SC24 are marked on the top panel.

Table 1 Solar cycles in the present study.

SC N°	SC start date (year-month)	SC peak date (year-month)	SC peak SSN	SC end date (year-month)
SC20	1964-10	1968-11	157	1976-02
SC21	1976-03	1979-12	233	1986-08
SC22	1986-09	1989-11	214	1996-07
SC23	1996-08	2001-11	180	2008-11
SC24	2008-12	2014-04	116	2019-12

for monthly and yearly mean data, respectively) with the SSN variation. This implies a significant enhancement in the CR flux during SC24. Average geomagnetic condition variations are depicted by the geomagnetic indices. In general, Dst represents the impacts of storm time ring currents around the geomagnetic equator (Sugiura, 1964), AE represents auroral electrojet activity related to substorms (Davis and Sugiura, 1966), and the ap index is a well accepted indicator for global-scale geomagnetic activity (Rostoker, 1972). During SC24, an overall decrease in geomagnetic activity compared to previous cycles could be recorded from these indices, which are consistent with previous reports (e.g. Grandin, Aikio, and Kozlovsky, 2019; Kakad et al., 2019).

Table 2 Comparison among solar cycles[a]. See text for the definition of the parameters.

	SC20	SC21	SC22	SC23	SC24
⟨SSN⟩ peak	149	192	213	180	113
HILDCAAs (HILDCAAs per year)	11	39 (3.5)	40 (4.0)	41 (3.4)	14 (1.6)
All storms (all storms per year)	207 (18.8)	323 (29.4)	308 (30.8)	282 (23.5)	159 (14.5)
Moderate storms (moderate storms per year)	162 (14.7)	242 (22.0)	218 (21.8)	202 (16.8)	137 (12.5)
Intense storms (intense storms per year)	43 (3.9)	77 (7.0)	81 (8.1)	71 (5.9)	22 (2.0)
Super storms (superstorms per year)	2 (0.2)	4 (0.4)	9 (0.9)	9 (0.8)	0 (0.0)
$\langle Bo \rangle$ peak (nT)	7	9	9	8	7
$\langle Vsw \rangle$ peak (km s^{-1})	525	476	527	543	455
$\langle D500 \rangle$ peak (%)	70	58	59	74	45
$\langle VBs \rangle$ peak (mV m^{-1})	0.40	0.48	0.44	0.38	0.32
$\langle \epsilon \rangle$ peak (10^{11} W)	1.81	2.67	3.11	2.24	1.56

[a]The values of the parameters represent the peak values of the yearly mean parameters in each solar cycle.

All geomagnetic storms and HILDCAA events during the period are identified. The HILDCAAs are identified, based on original criteria suggested by Tsurutani and Gonzalez (1987), as long intervals (2 days or longer) of intense auroral activity with peak AE > 1000 nT when AE does not fall below 200 nT for more than 2 h at a time. The Dst index was used to make sure that no magnetic storms occurred during the intervals. The Dst ≤ -50 nT criterion is used as a threshold for a magnetic storm (Gonzalez et al., 1994). The storms are further classified as moderate (-50 nT $\geq$ Dst > -100 nT), intense (-100 nT $\geq$ Dst > -250 nT), and superstorms (Dst ≤ -250 nT) based on the Dst peak intensity. Total numbers (and numbers per year) of HILDCAAs, magnetic storms of different intensity in each of the solar cycles are listed in Table 2. It should be noted that due to availability of high-resolution AE indices from 1975 on, the table contains only 1 year of HILDCAA observation for SC20. The peak values of the SSNs in each solar cycle based on yearly mean values are also shown. Table 2 confirms the lowest numbers of magnetic storms, HILDCAAs as well as their occurrence rates (numbers per year) during SC24 compared to previous cycles.

Figure 2 shows a superposed analysis of yearly occurrence rates of HILDCAAs and magnetic storms during each solar cycle. The zero epoch time corresponds to the SSN peak in each solar cycle, preceded by the ascending phase (from start to the peak) and followed by the descending phase (from peak to the end) of the cycle. The asymmetric distributions around the SSN peak are due to varying lengths of the descending and the ascending phases of the cycles (Table 1). Considering the above-mentioned binning process, SC24 had the longest ascending phase and the shortest descending phase compared to previous cycles (Figure 2, top panel and Table 1). While HILDCAAs can occur during any phase of a solar cycle, the occurrence rate is higher during the descending phase. This is in agreement with previous statistical results (e.g. Hajra et al., 2013, 2014a). Significant reduction in HILDCAA occurrence during SC24 can be noted from Figure 2 and Table 2. During SC24, HILDCAA rate reduced by $\approx 56\%$, $\approx 61\%$ and $\approx 54\%$ from that in SC21, SC22, and SC23, respectively.

Magnetic storm distributions are much more centered around the SSN maximum (Figure 2). While the solar maximum centric occurrence is most prominent for intense storms, moderate storms peak during the descending phase, resulting in an overall dual-peak occur-

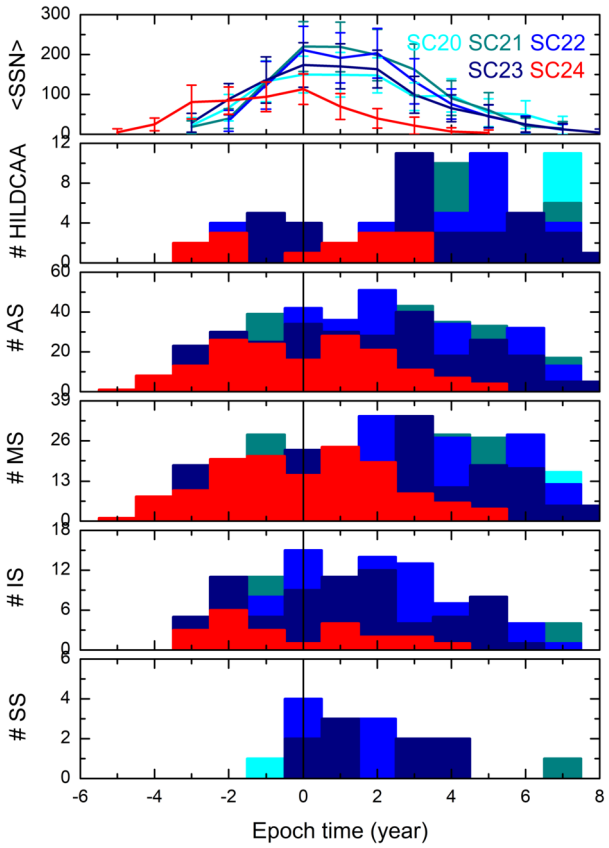

Figure 2 From top to bottom, the panels show the superposed epoch variations of yearly mean SSN (and standard deviations shown by horizontal bars), yearly numbers of HILDCAAs, all storms (AS), moderate storms (MS), intense storms (IS), and superstorms (SS), respectively from Solar Cycles 20 through 24. The zero epoch time corresponds to the SSN peak of the solar cycle.

rence pattern of magnetic storms (e.g. Tsurutani and Gonzalez, 1987; Gonzalez, Gonzalez, and Tsurutani, 1990; Gonzalez et al., 1994, 2011; Echer et al., 2004, 2008; Echer, Gonzalez, and Tsurutani, 2011; Hajra et al., 2013, 2014a,b, and the references therein). The lowest number of storms is recorded during SC24. Interestingly, it exhibited $\approx 15-34\%$ reduction in moderate storms, $\approx 49-75\%$ reduction in intense storms compared to previous cycles, and no superstorms.

Geomagnetic storms and HILDCAAs have different solar and interplanetary drivers. The strongest storms at the Earth are related to interplanetary coronal mass ejections (ICMEs) (e.g. Tsurutani et al., 1988; Gosling et al., 1990; Richardson, Cane, and Cliver, 2002; Echer et al., 2008), while HILDCAAs are associated with solar wind HSSs emanated from coronal holes and corotating interaction regions (CIRs) between fast and slow streams (Tsurutani and Gonzalez, 1987; Hajra et al., 2013; Souza et al., 2016; Mendes et al., 2017; Guarnieri et al., 2018; Marques de Souza et al., 2018; Tsurutani et al., 2019). In addition, ICMEs exhibit a solar cycle distribution similar to the storm distribution (see, Webb and Howard, 1994; Gopalswamy et al., 2004; Tsurutani et al., 2006; Obridko et al., 2012, and references therein). On the other hand, extension of the coronal holes to lower solar latitudes facilitates the CIR/HSS impacts on Earth during the declining phase and solar minimum. Recent works show significant reductions in ICMEs (e.g. Scolini et al., 2018; Lamy et al., 2019; Syed Ibrahim et al., 2019, and references therein) and equatorial coronal holes and, consequently, HSSs and CIRs (e.g. Grandin, Aikio, and Kozlovsky, 2019; Nakagawa, Nozawa,

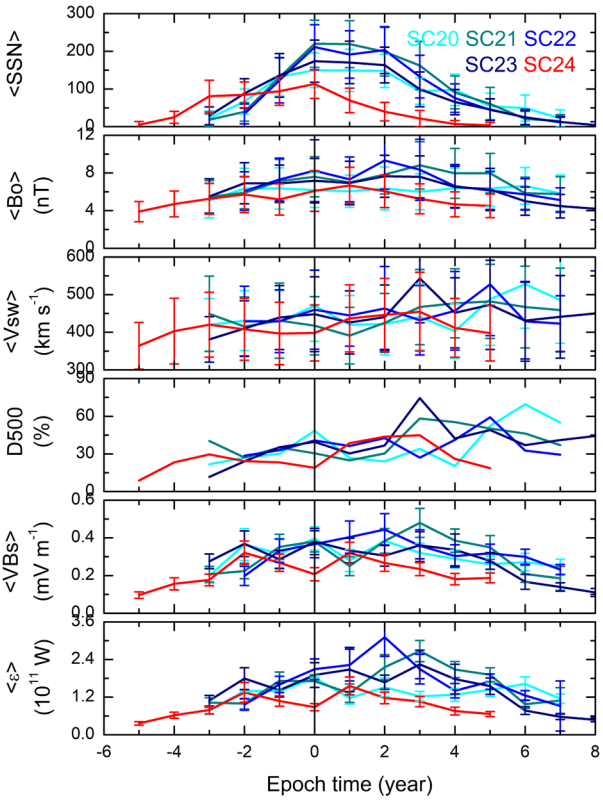

Figure 3 From top to bottom, the panels show the superposed epoch variations of yearly mean SSN, interplanetary magnetic field (IMF) Bo, Vsw, $D500$, VBs, and Akasofu ϵ-parameter, respectively during Solar Cycles 20 through 24. The horizontal bars show the standard deviations from the mean. The zero epoch time corresponds to the SSN peak of the solar cycle.

and Shinbori, 2019) in SC24, which are consistent with reductions in magnetic storms and HILDCAAs, respectively, reported in the present work.

Now, what is the impact of the above-mentioned reduction in solar and interplanetary drivers on the solar wind–magnetosphere coupling? This is investigated using solar wind and interplanetary parameters shown in Figure 3. Solar wind plasma and interplanetary magnetic field (IMF) data are collected from the OMNIWeb database (http://omniweb.gsfc.nasa.gov/) that is formed by time-shifting the data collected from the NASA's Advanced Composition Explorer (ACE), Wind, and Interplanetary Monitoring Platform 8 (IMP 8) spacecraft to the Earth's bow shock nose. The IMF vector components in geocentric solar magnetospheric (GSM) coordinates are used in this work. In GSM coordinates, the x-axis is directed towards the Sun and the y-axis is in the $\mathbf{\Omega}\times\hat{\mathbf{x}}/|\mathbf{\Omega}\times\hat{\mathbf{x}}|$ direction, where $\mathbf{\Omega}$ is aligned with the magnetic south pole axis of the Earth. The z-axis completes a right-hand system.

Figure 3 shows superposed analyses of yearly mean IMF magnitude ($\langle Bo\rangle$), plasma speed ($\langle Vsw\rangle$), yearly percentage of days with daily peak $Vsw \geq 500$ km s^{-1} (named as $D500$), coupling functions VBs, and Akasofu ϵ-parameter along with the standard deviations of the parameters from the mean values. The $D500$ is estimated as an indicator of the occurrence of solar wind HSSs. The VBs is the solar wind electric field where V represents the plasma or solar wind speed and Bs is the southward component of the IMF (Bs is zero in absence of a southward component). The VBs has shown to be the main driver of geomagnetic activity (e.g. Burton, McPherron, and Russell, 1975; Tsurutani et al., 1992; Finch, Lockwood, and Rouillard, 2008). The Akasofu ϵ-parameter ($\approx VswBo^2\ \sin^4(\theta/2)R_{CF}^2$) gives an approximate estimate of magnetospheric energy input rate (Perreault and Akasofu,

Table 3 Correlation coefficients (r) between the solar wind/interplanetary parameters and the geomagnetic activity indices, HILDCAAs, and geomagnetic storms of varying intensity for solar cycles from SC20 through SC24.

	⟨SSN⟩	⟨Bo⟩	⟨Vsw⟩	⟨$D500$⟩	⟨VBs⟩	⟨ϵ⟩
⟨Dst⟩	−0.63	−0.82	−0.38	−0.37	−0.72	−0.82
⟨ap⟩	0.59	0.84	0.54	0.51	0.80	0.90
⟨AE⟩	0.49	0.82	0.67	0.66	0.72	0.82
HILDCAA	−0.14	0.26	0.78	0.74	0.27	0.30
All storm	0.71	0.89	0.26	0.28	0.83	0.87
Moderate storm	0.56	0.78	0.28	0.32	0.72	0.74
Intense storm	0.76	0.84	0.13	0.12	0.79	0.85
Super storm	0.52	0.55	0.21	0.20	0.49	0.64

1978). Here θ is the IMF orientation clock angle, and R_{CF} is the Chapman–Ferraro magnetopause distance (Chapman and Ferraro, 1931; Shue and Chao, 2013). The peak values of the yearly mean parameters in each solar cycle are listed in Table 2.

In any solar cycle, while ⟨Vsw⟩ and $D500$ exhibit peaks during the declining phase (similar to HILDCAAs), distributions of ⟨Bo⟩ and coupling functions are centered around the SSN peak (similar to magnetic storms). As can be noted from the large standard deviations, all the solar wind/interplanetary parameters exhibit significant variability, from a few minutes to years. However, variation trends can be inferred from the yearly mean values. Compared to previous solar cycles, an overall reduction in the solar wind–interplanetary parameters and energy coupling can be noted in SC24 (Figure 3). Quantitatively, the reductions are $\approx 0-22\%$ in solar cycle peak ⟨Bo⟩, $\approx 5-16\%$ in peak ⟨Vsw⟩, $\approx 23-40\%$ in peak $D500$, $\approx 16-33\%$ in peak ⟨VBs⟩, and $\approx 14-50\%$ in peak ⟨ϵ⟩.

To understand the relative importance of the solar wind–magnetospheric coupling parameters in the reduction of geomagnetic activity, regression analysis is performed. Table 3 shows the correlation coefficients (r) between the solar wind/interplanetary parameters and the geomagnetic activity indices, HILDCAAs, and geomagnetic storms of varying intensity for solar cycles from SC20 through SC24.

As expected, HILDCAAs exhibit the strongest correlation with solar wind speed Vsw due to their association with HSSs and CIRs. On the other hand, geomagnetic storms and geomagnetic indices exhibit the strongest correlation with Akasofu ϵ-parameter and/or IMF Bo. Strong correlation between the ϵ-parameter and geomagnetic storms and indices may suggest that a reduction in ϵ-parameter, in general, in SC24 would cause a reduction in geomagnetic activity. However, the ϵ-parameter (containing a term Bo^2) is much more strongly dependent on the IMF than on Vsw. This is consistent with stronger correlation of geomagnetic activity with IMF Bo than with Vsw (Table 3). In addition, the reduction of IMF is a causal effect of the reduced solar activity that is a consequence of the reduction in solar photospheric magnetic fields as discussed before (e.g. Janardhan, Bisoi, and Gosain, 2010; Janardhan et al., 2015; Livingston, Penn, and Svalgaard, 2012; Sasikumar Raja et al., 2019).

3. Conclusions

The present work indicates a strong impact of the solar activity cycle magnitude on the solar wind–magnetosphere energy coupling and resultant geomagnetic activity. The weakest

magnitude of Solar Cycle 24 is found to be associated with an overall reduction in energy coupling and reduced numbers of magnetic storms and HILDCAAs. The stronger the storms, the stronger the reduction in number with no superstorms in Solar Cycle 24. This has a great impact on the cosmic ray shielding. As shown in the present work, reduced solar activity makes the near-Earth space exposed to a higher flux of cosmic rays. This can have important effects on manned missions at low Earth orbit or to the Moon and Mars.

Recent studies predict the solar activity entering in a period of grand minimum (e.g. Wang, 2017; Jiang and Cao, 2018; Upton and Hathaway, 2018; Gonçalves, Echer, and Frigo, 2020, and references therein). This may lead to a much lower solar wind energy input in the magnetosphere and a further decrease in geomagnetic activity events. This has large impacts on space weather effects and technological applications.

Acknowledgements The work is funded by the Science and Engineering Research Board (SERB), a statutory body of the Department of Science and Technology (DST), Government of India through a Ramanujan Fellowship. I would like to thank Prof. Bruce T. Tsurutani for helpful scientific discussions. I also thank the reviewer for extremely valuable suggestions that substantially improved the manuscript.

Disclosure of Potential Conflicts of Interest The author declares that he has no conflicts of interest.

References

Akasofu, S.-I.: 1964, The development of the auroral substorm. *Planet. Space Sci.* **12**, 273. DOI.

Burton, R.K., McPherron, R.L., Russell, C.T.: 1975, An empirical relationship between interplanetary conditions and *Dst*. *J. Geophys. Res.* **80**, 4204. DOI.

Chapman, S., Ferraro, V.C.A.: 1931, A new theory of magnetic storms. *Terr. Magn. Atmos. Electr.* **36**, 77. DOI.

Davis, T.N., Sugiura, M.: 1966, Auroral electrojet activity index *AE* and its universal time variations. *J. Geophys. Res.* **71**, 785. DOI.

Dungey, J.W.: 1961, Interplanetary magnetic field and the auroral zones. *Phys. Rev. Lett.* **6**, 47. DOI.

Echer, E., Gonzalez, W.D., Tsurutani, B.T.: 2011, Statistical studies of geomagnetic storms with peak Dst ≤ -50 nT from 1957 to 2008. *J. Atmos. Solar-Terr. Phys.* **73**, 1454. DOI.

Echer, E., Gonzalez, W.D., Gonzalez, A.L.C., Prestes, A., Vieira, L.E.A., Dal Lago, A., Guarnieri, F.L., Schuch, N.J.: 2004, Long-term correlation between solar and geomagnetic activity. *J. Atmos. Solar-Terr. Phys.* **66**, 1019. DOI.

Echer, E., Gonzalez, W.D., Tsurutani, B.T., Gonzalez, A.L.C.: 2008, Interplanetary conditions causing intense geomagnetic storms ($Dst < -100$ nT) during Solar Cycle 23 (1996–2006). *J. Geophys. Res.* **113**, 1. DOI.

Finch, I.D., Lockwood, M.L., Rouillard, A.P.: 2008, Effects of solar wind magnetosphere coupling recorded at different geomagnetic latitudes: separation of directly-driven and storage/release systems. *Geophys. Res. Lett.* **35**, L21105. DOI.

Gonçalves, Í.G., Echer, E., Frigo, E.: 2020, Sunspot cycle prediction using warped Gaussian process regression. *Adv. Space Res.* **65**, 677. DOI.

Gonzalez, W.D., Gonzalez, A.L.C., Tsurutani, B.T.: 1990, Dual-peak solar cycle distribution of intense geomagnetic storms. *Planet. Space Sci.* **38**, 181.

Gonzalez, W.D., Mozer, F.S.: 1974, A quantitative model for the potential resulting from reconnection with an arbitrary interplanetary magnetic field. *J. Geophys. Res.* **79**, 4186. DOI.

Gonzalez, W.D., Joselyn, J.A., Kamide, Y., Kroehl, H.W., Rostoker, G., Tsurutani, B.T., Vasyliunas, V.M.: 1994, What is a geomagnetic storm? *J. Geophys. Res.* **99**, 5771. DOI.

Gonzalez, W.D., Echer, E., Tsurutani, B.T., Gonzalez, A.L., Lago, A.: 2011, Interplanetary origin of intense, superintense and extreme geomagnetic storms. *Space Sci. Rev.* **158**, 69. DOI.

Gopalswamy, N., Nunes, S., Yashiro, S., Howard, R.A.: 2004, Variability of solar eruptions during cycle 23. *Adv. Space Res.* **34**, 391. DOI.

Gosling, J.T., Bame, S.J., McComas, D.J., Phillips, J.L.: 1990, Coronal mass ejections and large geomagnetic storms. *Geophys. Res. Lett.* **17**, 901. DOI.
Grandin, M., Aikio, A.T., Kozlovsky, A.: 2019, Properties and geoeffectiveness of solar wind high-speed streams and stream interaction regions during Solar Cycles 23 and 24. *J. Geophys. Res.* **124**, 3871. DOI.
Guarnieri, F.L., Tsurutani, B.T., Vieira, L.E.A., Hajra, R., Echer, E., Mannucci, A.J., Gonzalez, W.D.: 2018, A correlation study regarding the AE index and ACE solar wind data for Alfvénic intervals using wavelet decomposition and reconstruction. *Nonlinear Process. Geophys.* **25**, 67. DOI.
Hajra, R., Tsurutani, B.T., Lakhina, G.S.: 2020, The complex space weather events of 2017 September. *Astrophys. J.* **899**, 3. DOI.
Hajra, R., Echer, E., Tsurutani, B.T., Gonzalez, W.D.: 2013, Solar cycle dependence of High-Intensity Long-Duration Continuous AE Activity (HILDCAA) events, relativistic electron predictors? *J. Geophys. Res.* **118**, 5626. DOI.
Hajra, R., Echer, E., Tsurutani, B.T., Gonzalez, W.D.: 2014a, Superposed epoch analyses of HILDCAAs and their interplanetary drivers: solar cycle and seasonal dependences. *J. Atmos. Solar-Terr. Phys.* **121**, 24. DOI.
Hajra, R., Echer, E., Tsurutani, B.T., Gonzalez, W.D.: 2014b, Solar wind-magnetosphere energy coupling efficiency and partitioning: HILDCAAs and preceding CIR storms during Solar Cycle 23. *J. Geophys. Res.* **119**, 2675. DOI.
Ingale, M., Janardhan, P., Bisoi, S.K.: 2019, Beyond the minisolar maximum of Solar Cycle 24: declining solar magnetic fields and the response of the terrestrial magnetosphere. *J. Geophys. Res.* **124**, 6363. DOI.
Janardhan, P., Bisoi, S.K., Gosain, S.: 2010, Solar polar fields during cycles 21 – 23: correlation with meridional flows. *Solar Phys.* **267**, 267. DOI.
Janardhan, P., Bisoi, S.K., Ananthakrishnan, S., Tokumaru, M., Fujiki, K., Jose, L., Sridharan, R.: 2015, A 20 year decline in solar photospheric magnetic fields: inner-heliospheric signatures and possible implications. *J. Geophys. Res.* **120**, 5306. DOI.
Janardhan, P., Fujiki, K., Ingale, M., Bisoi, S.K., Rout, D.: 2018, Solar cycle 24: an unusual polar field reversal. *Astron. Astrophys.* **618**, A148. DOI.
Jiang, J., Cao, J.: 2018, Predicting solar surface large-scale magnetic field of cycle 24. *J. Atmos. Solar-Terr. Phys.* **176**, 34. DOI.
Kakad, B., Kakad, A., Ramesh, D.S., Lakhina, G.S.: 2019, Diminishing activity of recent solar cycles (22 – 24) and their impact on geospace. *J. Space Weather Space Clim.* **9**, A1. DOI.
Lamy, P.L., Floyd, O., Boclet, B., Wojak, J., Gilardy, H., Barlyaeva, T.: 2019, Coronal mass ejections over Solar Cycles 23 and 24. *Space Sci. Rev.* **215**, 39. DOI.
Livingston, W., Penn, M.J., Svalgaard, L.: 2012, Decreasing sunspot magnetic fields explain unique 10.7 cm radio flux. *Astrophys. J.* **757**, L8. DOI.
Marques de Souza, A., Echer, E., Bolzan, M.J.A., Hajra, R.: 2018, Cross-correlation and cross-wavelet analyses of the solar wind IMF B_Z and auroral electrojet index AE coupling during HILDCAAs. *Ann. Geophys.* **36**, 205. DOI.
Mendes, O., Domingues, M.O., Echer, E., Hajra, R., Menconi, V.E.: 2017, Characterization of high-intensity, long-duration continuous auroral activity (HILDCAA) events using recurrence quantification analysis. *Nonlinear Process. Geophys.* **24**, 407. DOI.
Nakagawa, Y., Nozawa, S., Shinbori, A.: 2019, Relationship between the low-latitude coronal hole area, solar wind velocity, and geomagnetic activity during Solar Cycles 23 and 24. *Earth Planets Space* **71**, 24. DOI.
Obridko, V.N., Ivanov, E.V., Özgüç, A., Kilcik, A., Yurchyshyn, V.B.: 2012, Coronal mass ejections and the index of effective solar multipole. *Solar Phys.* **281**, 779. DOI.
Ohtani, S.: 2001, Substorm trigger processes in the magnetotail: recent observations and outstanding issues. *Space Sci. Rev.* **95**, 347. DOI.
Perreault, P., Akasofu, S.-I.: 1978, A study of geomagnetic storms. *Geophys. J. Roy. Astron. Soc.* **54**, 547. DOI.
Richardson, I.G., Cane, H.V., Cliver, E.W.: 2002, Sources of geomagnetic activity during nearly three solar cycles (1972 – 2000). *J. Geophys. Res.* **107**, SSH 8-1. DOI.
Rostoker, G.: 1972, Geomagnetic indices. *Rev. Geophys.* **10**, 935. DOI.
Sasikumar Raja, K., Janardhan, P., Bisoi, S.K., Ingale, M., Subramanian, P., Fujiki, K., Maksimovic, M.: 2019, Global solar magnetic field and interplanetary scintillations during the past four solar cycles. *Solar Phys.* **294**, 123. DOI.
Scolini, C., Messerotti, M., Poedts, S., Rodriguez, L.: 2018, Halo coronal mass ejections during Solar Cycle 24: reconstruction of the global scenario and geoeffectiveness. *J. Space Weather Space Clim.* **8**, A09. DOI.

Shue, J.-H., Chao, J.-K.: 2013, The role of enhanced thermal pressure in the earthward motion of the Earth's magnetopause. *J. Geophys. Res.* **118**, 3017. DOI.

Souza, A.M., Echer, E., Bolzan, M.J.A., Hajra, R.: 2016, A study on the main periodicities in interplanetary magnetic field Bz component and geomagnetic AE index during HILDCAA events using wavelet analysis. *J. Atmos. Solar-Terr. Phys.* **149**, 81. DOI.

Sugiura, M.: 1964, Hourly values of equatorial Dst for the IGY. *Ann. Int. Geophys. Year* **35**, 9.

Syed Ibrahim, M., Joshi, B., Cho, K.-S., Kim, R.-S., Moon, Y.-J.: 2019, Interplanetary coronal mass ejections during Solar Cycles 23 and 24: Sun–Earth propagation characteristics and consequences at the near-Earth region. *Solar Phys.* **294**, 54. DOI.

Tsurutani, B.T., Echer, E., Gonzalez, W.D.: 2011, The solar and interplanetary causes of the recent minimum in geomagnetic activity (MGA23): a combination of mid latitude small coronal holes, low IMF B_Z variances, low solar wind speeds and low solar magnetic fields. *Ann. Geophys.* **29**, 839. DOI.

Tsurutani, B.T., Gonzalez, W.D.: 1987, The cause of high-intensity long-duration continuous AE activity (HILDCAAs): interplanetary Alfvén wave trains. *Planet. Space Sci.* **35**, 405. DOI.

Tsurutani, B.T., Lakhina, G.S., Hajra, R.: 2020, The physics of space weather/solar-terrestrial physics (STP): what we know now and what the current and future challenges are. *Nonlinear Process. Geophys.* **27**, 75. DOI.

Tsurutani, B.T., Meng, C.-I.: 1972, Interplanetary magnetic-field variations and substorm activity. *J. Geophys. Res.* **77**, 2964. DOI.

Tsurutani, B.T., Gonzalez, W.D., Tang, F., Akasofu, S.I., Smith, E.J.: 1988, Origin of interplanetary southward magnetic fields responsible for major magnetic storms near solar maximum (1978 – 1979). *J. Geophys. Res.* **93**, 8519. DOI.

Tsurutani, B.T., Gonzalez, W.D., Tang, F., Lee, Y.T.: 1992, Great magnetic storms. *Geophys. Res. Lett.* **19**, 73. DOI.

Tsurutani, B.T., Gonzalez, W.D., Gonzalez, A.L.C., Guarnieri, F.L., Gopalswamy, N., Grande, M., Kamide, Y., Kasahara, Y., Lu, G., Mann, I., McPherron, R., Soraas, F., Vasyliunas, V.: 2006, Corotating solar wind streams and recurrent geomagnetic activity: a review. *J. Geophys. Res.* **111**, A07S01. DOI.

Tsurutani, B.T., Hajra, R., Echer, E., Lakhina, G.S.: 2019, Comment on "First observation of mesosphere response to the solar wind high-speed streams" by W. Yi et al. *J. Geophys. Res.* **124**, 8165. DOI.

Upton, L.A., Hathaway, D.H.: 2018, An updated Solar Cycle 25 prediction with AFT: the modern minimum. *Geophys. Res. Lett.* **45**, 8091. DOI.

Wang, Y.-M.: 2017, Surface flux transport and the evolution of the Sun's polar fields. *Space Sci. Rev.* **210**, 351. DOI.

Webb, D.F., Howard, R.A.: 1994, The solar cycle variation of coronal mass ejections and the solar wind mass flux. *J. Geophys. Res.* **99**, 4201. DOI.